The phenomenon of Alfvénic vortex shedding

M. Gruszecki,[1,*] V.M. Nakariakov,[1] T. Van Doorsselaere,[1] and T.D. Arber[1]

[1] *Centre for Fusion, Space and Astrophysics, Department of Physics, University of Warwick, Coventry CV4 7AL, United Kingdom*

Generation of Alfvénic vortices by the interaction of compressible plasma flows with field-aligned blunt obstacles is modelled in terms of magnetohydrodynamics. It is found that periodic shedding of vortices with opposite vorticity is a robust feature of the interaction in a broad range of plasma parameters: for plasma-beta from 0.025 to 0.5, and for the flow speeds from 0.1 to 0.99 of the fast magnetoacoustic speed. The Strouhal number is found to be consistently in the range 0.15-0.25 in the whole range of parameters. The induced Alfvénic vortices are compressible and contain spiral-armed perturbations of the magnetic field strength and plasma mass density up to 50-60% of the background values. The generated electric current also has the spiral-armed structuring.

PACS numbers: 52.30.Cv, 52.35.We, 52.65.Kj, 95.30.Qd

It is well known that the interaction of a flow with a non-moving bluff body results in a so called *Kármán vortex street*, where vortices with opposite vorticity are periodically generated alternating from either side of the blunt body in the downstream region, e.g. [1, 2]. The phenomenon of periodic shedding of hydrodynamic vortices has many consequences in oceanography, atmospheric physics and engineering. The phenomenon can be considered as an example of auto-oscillations, when a steady energy supply causes an oscillatory behaviour of the dynamical system.

The effect of vortex shedding in a magnetised medium is less well understood. It is known to play a role in a number of applications and physical situations. For example, in industrial magentohydrodynamics (MHD) the effect of MHD vortex shedding can be used for the leveling the temperature by convective transport in liquid metals, e.g. [3]. In controlled fusion, this effect is studied in association with the formation of coherent structures (blobs) in the scrape-off layer of tokamak plasmas [4] In geophysics, the observed rocking of the floating bubbles in the equatorial ionospheric F-region is attributed to this effect [5]. Similarly, a zigzag path of magnetic flux tubes emerging in the solar interior, caused by vortex shedding, has been found in numerical simulations [6]. Also, this effect has been found to accompany the impulsive plasmoid penetration of the magnetosphere [7]. Also, the size of the vortices generated by the interaction of the solar wind with the Earth is important in the context of the solar-wind/magnetosphere coupling [8]. Strong vortex shedding has been observed coincident with disruption and reformation of the termination shock in MHD simulations of astrophysical jets [9]. There is a growing interest to Alfvénic vortices and their generation in the magnetopause and magnetosheath, e.g. [10, 11]. Recently, periodic shedding of Alfvénic vortices was suggested as a mechanism for the excitation of kink oscillations of plasma loops in the solar corona [12].

The quantitative characteristics of the vortex shedding phenomenon is the Strouhal number (St) that is a dimensionless parameter constructed from the period of the vortex shedding, the size of the blunt body and the flow velocity. In hydrodynamics, the typical value of the Strouhal number that describes the interaction of a steady flow with a cylindrical obstacle of a circular cross-section is in the range from 0.15 to 0.2 [2]. In magnetised fluids and plasmas, there has not been a systematic and detailed studies of this parameter. In some studies the Strouhal number has been estimated. For example, in the numerical experiments on the magnetohydrodynamic flows of liquid metals [3] the Strouhal number was found to be about 0.2. In the Earth's magnetospheric plasma, the Strouhal number has experimentally been estimated as 0.3 [13]. Theoretically, in the case of MHD, the consideration of the plasma motion in the plane perpendicular to the magnetic field is governed by the gradients of the total, magnetic and gas, pressure. These pressures have different dependence upon the mass density. In the adiabatic case the gas pressure is proportional to the density to $\gamma = 5/3$, while the magnetic pressure depends upon the density squared. Thus, the consideration of the MHD flows requires both terms are explicitly included, i.e. it can not be determined from a simple rescaling of results from not-magnetised fluid [14].

The aim of this Letter is to present the parametric numerical study of the interaction of a steady plasma flow with a cylindrical obstacle in the MHD regime, and to determine the dependence of the Strouhal number upon the plasma properties.

*Electronic address: M.Gruszecki@warwick.ac.uk

Our governing equations are the compressible magne-

tohydrodynamic (MHD) equations,

$$\frac{\partial \varrho}{\partial t} + \nabla \cdot (\varrho \mathbf{V}) = 0, \quad (1)$$

$$\varrho \frac{\partial \mathbf{V}}{\partial t} + \varrho(\mathbf{V} \cdot \nabla)\mathbf{V} = -\nabla p + \frac{1}{\mu}(\nabla \times \mathbf{B}) \times \mathbf{B}, \quad (2)$$

$$\frac{\partial \mathbf{B}}{\partial t} = \nabla \times (\mathbf{V} \times \mathbf{B}), \quad (3)$$

$$\varrho \frac{\partial \varepsilon}{\partial t} + \varrho \mathbf{V} \nabla \varepsilon = -p \nabla \cdot \mathbf{V}, \quad (4)$$

$$\nabla \cdot \mathbf{B} = 0, \quad (5)$$

where ϱ is the mass density, p is the gas pressure, $\mathbf{B}$ is the magnetic field, $\mathbf{V} = [V_\mathbf{x}, V_\mathbf{y}, V_\mathbf{z}]$ is the flow velocity; and μ is the magnetic permeability and ε is the specific internal energy density, $p = \varrho\varepsilon(\gamma - 1)$ and $\gamma = 5/3$ is the ratio of specific heats. We limit our discussion to a 2.5-D dynamics: all variables are taken to be invariant in the y-direction, $\partial/\partial y = 0$, while y-components of the magnetic field and velocity vectors are not necessarily zero. Some potentially important effects, e.g. dispersion and drift multi-fluid effects, are missing in the governing equations. However, in a number of applications, the characteristic scales of the vortices are much greater than the spatial scales at which those effects become important. For example, a typical diameter of a coronal plasma loop that can act as an obstacle exceeds a thousand of km, while the proton gyroradius is several hundred meters. Hence, the application of the MHD equations is well justified.

We consider an equilibrium which corresponds to the interaction of an initially uniform and steady plasma flow with a cylindrical blunt body. The axis of the cylinder is chosen in the y-direction. Initially, both mass density and the magnetic field are uniform over the whole space around the blunt body. The magnetic field is directed along the y-axis, parallel to the blunt body axis. Thus, the initial, equilibrium plasma quantities are given by the following expressions,

$$p(x,z), \varrho(x,z), B\hat{\mathbf{y}} = \begin{cases} p_0, \varrho_\mathrm{i}, B_0, & x^2 + z^2 \le d^2/4, \\ p_0, \varrho_\mathrm{e}, B_0, & x^2 + z^2 > d^2/4, \end{cases}$$

where $\hat{\mathbf{y}}$ is the unit vector of the y axis and d is the diameter of the cylinder. To exclude effects of the cylinder deformation and instability we set and keep fixed inside the cylinder $\mathbf{V}(x,z) = 0$. To initiate phenomenon of vortex shedding everywhere outside the cylinder we set homogeneous flow in x-component of velocity $V_\mathbf{x}$. The specific quantitative values of the initial equilibrium are taken to be consistent with the typical parameters of the solar coronal plasma (see Table I). However, the results obtained can be easily applied to other relevant plasma systems by straightforward renormalisation.

Equations (1-5) are numerically solved with the use of the Lagrangian-remap code Lare2d [15]. In our studies we simulate the plasma dynamics in a domain $(-50, 50) \times (-25, 25)$ Mm covered by 6500×2500 grid points, with the field-aligned cylindrical body being situated at the point (0, 0). We performed grid convergence studies to check the numerical results. We set zero gradients boundary conditions at all sides of the simulation box, allowing a propagating perturbation signal to leave freely, without reflection.

TABLE I: Parameters of the initial numerical equlibrium.

ϱ_0 [kg/m^3]	p_0 [Pa]	B_0 [T]	T_0 [K]	c_s [Mm/s]	V_A [Mm/s]	β
10^{-12}	10^{-2}	10^{-3}	$6 \cdot 10^5$	0.129	0.892	0.025

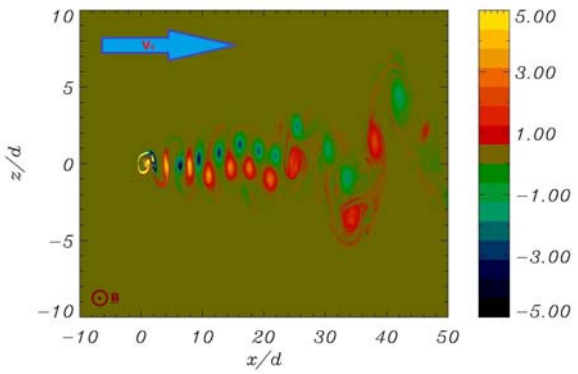

FIG. 1: Normalised profile of the vorticity $\omega \cdot d/V_0$ at $t = 220$ s for the case of the $V_0 = 0.3$ Mm/s. Spatial coordinates x and z are measured in units of diameter of the cylinder $d = 1$ Mm.

Figure 1 shows a typical snapshot of the von Karman vortex street, generated by the interaction of the steady flow with the cylinder situated at the (0,0) point. The phenomenon of vortex shedding is clearly seen: vortices of the opposite vorticity are alternatively and periodically generated on the opposite sides of the blunt body and then dragged with the flow downstream. The vortices can be considered as Alfvénic as shearing perturbations of the magnetic field occur in the direction perpendicular to the ambient magnetic field. The generated flow vorticity is parallel to the magnetic field.

We performed a series of numerical experiments, studying the effects of the cylinder diameter, plasma parameter β and the steady flow speed on the phenomenon. Both sub-Alfvénic and super-Alfvénic speeds were considered, while in all cases the flow speed remained lower than the fast magnetoacoustic speed. When the flow speed exceeds the characteristic speed of the information transfer across the magnetic field in the plasma, the fast magnetoacoustic speed, $(c_s^2 + V_A^2)^{1/2}$, the interaction changes qualitatively, as the shocks are formed. The latter regime is not considered in this study.

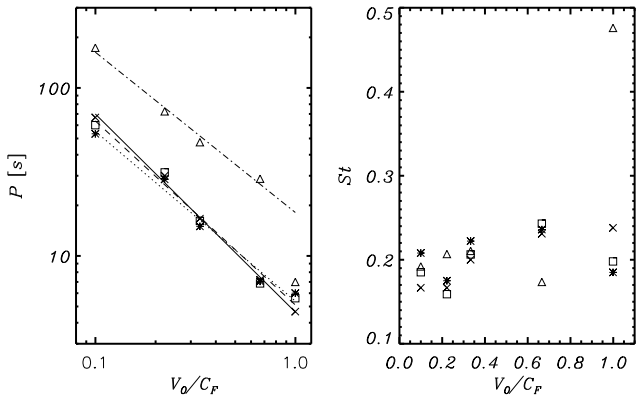

FIG. 2: The variation of the period P of Alfvénic vortex shedding (left panel) and the Strouhal number St (right panel) with the incoming flow speed V_0. The speed is measured in units of the equilibrium fast magnetoacoustic speed $C_{\rm F}$. The stars shows the results obtained for the cylinder with diameter $d = 1$ Mm, and the triangles for $d = 3$ Mm, and $\beta = 0.025$; the squares and crosses corresponds to $\beta = 0.1$ and $\beta = 0.5$, respectively, for $d = 1$ Mm. The gradients of the best-fitting straight lines are -1.17 (solid line), -1.01 (dotted line), -1.1 (dashed line) and -0.95 (dash-dotted line).

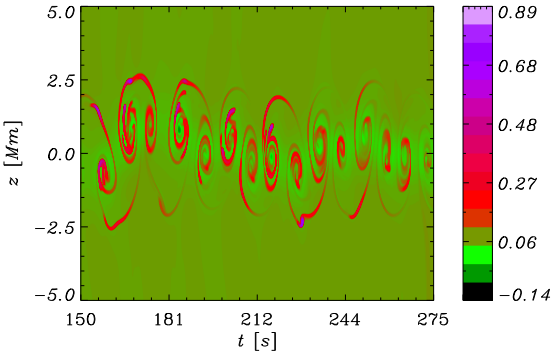

FIG. 3: Time-distance signatures of the normalised mass density variations in the generated street of Alfvénic vortices, $(\varrho(t) - \varrho(t = 0s))/\varrho(t = 0s)$, collected at $x = 8$ Mm.

Figure 2 shows the dependence of the Alfvénic vortex shedding period P upon the flow speed V_0 for different diameters d and the plasma β ranging from 0.025 to 0.5. One of the aims of this study is to test the hydrodynamic relation,

$$\frac{d}{PV_0} = \mathrm{St}, \qquad (6)$$

where the constant St is the Strouhal number in the MHD regime. The dependence of the Strouhal number, calculated according to equation (6) upon the flow speed is shown in the right panel of Fig. 2. In the calculations, the power-law dependence of the period upon the speed was determined by best-fitting the experimental dependence in the log-log plot with a linear function, using the least-square method (Fig. 2, left panel). The gradients of the approximating straight lines for all combinations of the parameters are found to be close to -1, hence $\log P \propto -\log(V_0)$. Thus, the scaling given by equation (6) is confirmed to take place in the MHD regime. It is established that the Strouhal number is almost independent of the flow speed and is consistently in the range 0.15-0.25. The abnormal value of St corresponding to the flow speed of about unity in one of the experiments is attributed to flows locally exceeding the magnetoacoustic speed. The results are found to be independent of the plasma β.

Figure 3 shows time-distance signatures of the perturbed mass density $(\varrho(t) - \varrho(t = 0))/\varrho(t = 0)$, collected at $x = 8$ Mm along the z-axis from the instant of time when the first vortex is reaching the observational point. The vortices are clearly visible in the mass density perturbations. For all vortices we see decreases in density towards their centres (see also Fig. 5). The dependence of the extreme values of the perturbations of the mass density, and the absolute values of the magnetic field and electric current density in the generated von Karman street upon the value of the incoming flow speed is shown in Figure 4. The estimations are based upon the use of five vortices in the street. The decrease in the mass density of the plasma at the vortex centre reaches about 10%. In the vortex periphery, the density is enhanced by up to 50-70%. Thus, the vortices are essentially compressible. Hence, strictly speaking, they should be called as fast magnetoacoustic [see 16, for a detailed discussion]. However, we shall keep using the established terminology and call them Alfvénic. The gas pressure perturbation, not shown here, exhibits a very similar shape.

The vortex diameter is measured as a distance between the points where the vorticity ω was two times larger than in vortex centre. To estimate it we used the vortex which reached the point $x/d \simeq 10$. The size of the generated Alfvénic vortices is found to be the same order of magnitude as the size of the blunt body (Fig. 4, last panel), similar to hydrodynamics.

Figure 5 shows zoomed contour plots of the internal structure of a vortex. The mass density and the magnetic field at the vortex centre are decreased. The transverse gradients in the magnetic field generate the current density according to the Ampere's law $\mathbf{j} = \nabla \times \mathbf{B}/\mu$. The induced current is clearly filamented, with individual current sheets having the structure of spiral arms. Similar structuring is seen in the density, vorticity and the magnetic field. Generation of such filamentary arms have been also observed e.g. in numerical experiments on the excitation of torsional Alfvén waves by a rapidly spinning rotor embedded in a magnetised plasma [17].

In conclusion, we have numerically studied the interac-

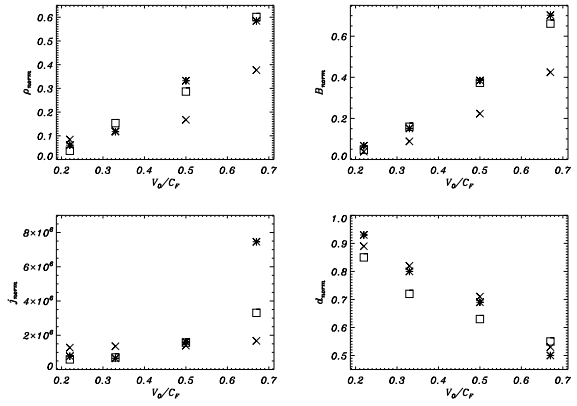

FIG. 4: Normalised minimum value of density $\varrho_{norm} = |(\varrho - \varrho_0)/\varrho_0|$ (top left panel), minimum value of magnetic induction $B_{norm} =| (B - B_0)/B_0 |$ (top right panel), maximum value of electric current $j_{norm} = j \cdot d/B_0$ (bottom left panel) and vortex diameter $d_{norm} = d_{vortex}/d$ (bottom right panel) as functions of the flow speed. The speed is measured in units of fast speed $C_{\rm F}$. The stars, squares and crosses corresponds to $\beta = 0.025$, $\beta = 0.1$ and $\beta = 0.5$, respectively.

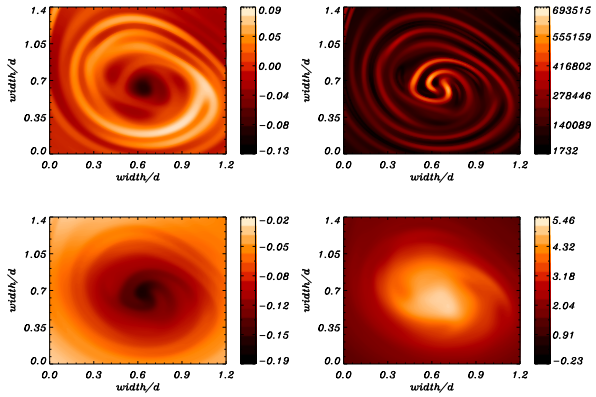

FIG. 5: Internal structure of an Alfvénic vortex: the mass density $(\varrho - \varrho_0)/\varrho_0$ (top left panel), the absolute values of the electric current density $j \cdot d/B_0$ (top right panel), magnetic field $(B - B_0)/B_0$ (bottom left panel) and vorticity $\omega_{norm} = \omega \cdot d/V_0$ (bottom right panel).

tion of steady uniform flow of a magnetised compressible plasma with an obstacle body of a cylindrical shape. It was found that this process leads to the periodic generation of Alfvénic vortices, which form a characteristic von Karman street. The Strouhal number is about 0.2 for a broad range of the speeds and the ratios of the gas and magnetic pressures in the plasma. Thus, as in hydrodynamics, the Strouhal number is a robust feature of the considered phenomenon in the case of rarified (e.g. space, astrophysical and laboratory) plasmas and can be used for plasma diagnostic. The generated vortices are essentially compressible, with the mass density perturbation up to 50-70% of the ambient value. The mass density perturbation in the vortices is accompanied by the perturbation of a similar strength of the absolute value of the magnetic field. Both mass density and magnetic field perturbations have a shape of filamentary spiral arms. The induced electric current has a similar structure. The steep gradients of the current density in the generated vortices are the preferential sites for magnetic reconnection and charged particle acceleration, and hence have implications for plasma heating, cross-field transport and EM wave emission.

MG is supported by the Newton International Fellowship NF090143. TVD acknowledges funding from the EC FP7 (FP7/2007-2013) under grant agreement number 220555.

[1] D.J. Tritton, *Physical Fluid Dynamics* (Van Nostrand, Princeton, 1977), 1st ed.
[2] C.H.K. Williamson, Ann. Rev. Fluid Mech. **28**, 477 (1996).
[3] V. Dousset, A. Pothérat, Phys. Fluids **20**, 017104 (2008).
[4] A. Y. Aydemir, Phys. Plasmas **12**, 062503 (2005).
[5] E. Ott, J. Geophys. Res. **83**, 2066 (1978).
[6] T. Emonet, F. Moreno-Insertis, M. Rast, Astrophys. J. **549**, 1212 (2001).
[7] J. D. Huba, J. Geophys. Res. **101**, 24855 (1996).
[8] J. E. Borovsky, Phys. Plasmas **13**, 056505 (2006)
[9] J. D. Huba, Astrophys. J. **512**, 105 (1999)
[10] O. Alexandrova, A. Mangeney, M. Maksimovic, N. Cornilleau-Wehrlin, J.-M. Bosqued, M. André, J. Geophys. Res. **111**, 12208 (2006).
[11] C. Foullon, C. J. Farrugia, A. N. Fazakerley, C. J. Owen, F. T. Gratton, F. T.; R. B. Torbert, J. Geophys. Res. **113**, A11203 (2008).
[12] V.M. Nakariakov, M.J. Aschwanden and T. Van Doorsselaere, Astron. Astrophys. **502**, 661 (2009).
[13] Z. A. Kereselidze, V. S. Orvelashvili, Geomagnetizm i Aeronomiia **27**, 165 (1987).
[14] L.D. Landau, E.M. Lifshitz, *Electrodynamics of continuous media* (Butterworth-Heinemann, 1995), 2nd ed.
[15] T. Arber, A.W. Longbottom, C.L. Gerrard and A.M. Milne, J. Comput. Phys. **171**, 151 (2001).
[16] T. Van Doorsselaere, V.M. Nakariakov, E. Verwichte, Astrophys. J. **676** L73 (2008).
[17] D. S. Balsara, D. S. Spicer, J. Comput. Phys. **149** 270 (1999).